



HAL
open science

A (NiMnCo)-Metal-Organic Framework (MOF) as active material for Lithium-ion battery electrodes

Marine Cognet, Thibaut Gutel, David Peralta, Jerome Maynadié, J Cambedouzou, Michaël Carboni, Daniel Meyer

► To cite this version:

Marine Cognet, Thibaut Gutel, David Peralta, Jerome Maynadié, J Cambedouzou, et al.. A (NiMnCo)-Metal-Organic Framework (MOF) as active material for Lithium-ion battery electrodes. Science and Technology for Energy Transition, 2023, Synthesis and characterisation of porous materials for clean energy application, 78, pp.33. 10.2516/stet/2023031 . cea-04290926

HAL Id: cea-04290926

<https://cea.hal.science/cea-04290926v1>

Submitted on 17 Nov 2023


HAL is a multi-disciplinary open access archive for the deposit and dissemination of scientific research documents, whether they are published or not. The documents may come from teaching and research institutions in France or abroad, or from public or private research centers.

L'archive ouverte pluridisciplinaire **HAL**, est destinée au dépôt et à la diffusion de documents scientifiques de niveau recherche, publiés ou non, émanant des établissements d'enseignement et de recherche français ou étrangers, des laboratoires publics ou privés.



Distributed under a Creative Commons Attribution 4.0 International License

A (NiMnCo)-Metal-Organic Framework (MOF) as active material for Lithium-ion battery electrodes

Marine Cagnet¹, Thibaut Gutel², David Peralta^{2,*} , Jerome Maynadié¹, Julien Cambedouzou¹, Michaël Carboni^{1,*}, and Daniel Meyer¹

¹ICSM, Univ Montpellier, CEA, CNRS, ENSCM, Marcoule, France

²Univ Grenoble Alpes, CEA, LITEN, DEHT, LM, 38000 Grenoble, France

Received: 24 April 2023 / Accepted: 10 October 2023

Abstract. A (NiMnCo)-Metal-Organic Framework and its oxidized and pyrolysed derivatives have been tested as electrode materials for lithium-ion batteries. Materials have been fully characterized by Scanning Electron Microscopy (SEM), powder X-Ray Diffraction (XRD), Thermogravimetric Analyses (TGA), Infrared (IR) spectroscopy and electrochemical properties have been determined in coin cells using lithium metal as the counter electrode. Studies have revealed specific capacities of 860 mAh g⁻¹ and 800 mAh g⁻¹ at 15 mA g⁻¹ respectively for the MOF and the oxide (690 and 190 mAh g⁻¹ after 50 cycles) whereas the corresponding pyrolysed compound has shown limited electrochemical performances. *Ex situ* XRD has been performed to highlight the evolution of the material structure during cycling. These results show that electrochemical storage is based on a conversion reaction.

Keywords: Metal-Organic Frameworks (MOFs), Li-Ion battery, Cathode active materials, Multimetalllic MOF, Energy storage.

1 Introduction

Energy storage is one of the biggest challenges for the next decades [1]. Energy consumption has never been so high, predictions show a dramatic increase in energy demand due to the economic growth and the expansion of populations [2]. There is a real need for an alternative to replace the dominant energy for a cleaner and more efficient development of our society. The management of renewable energy production through efficient electrochemical energy storage devices has become a priority because these energies are intermittent and need storage capacities to be massively included in large-scale power grids. To generate a new sustainable energy supply, battery properties must be improved in terms of capacity, security and durability [3].

In recent years, Li-ion Batteries (LiBs) have been developed and successfully commercialized for portable devices such as smartphones or laptops and more recently for electric vehicles [4]. Those batteries are usually composed of a positive electrode containing metal oxides, a negative one made of graphite, an organic electrolyte and a separator. LiBs have high energy density and good cyclability

compared to other commercial batteries. There are several generations of LiBs depending on the chemical composition of the electrode material [5]. Transition metals have been extensively used as cathode components in LiBs due to the reversible insertion/disinsertion of Li during the redox phenomena of the discharge/charge process as demonstrated by Mizushima *et al.* in the early 1980s [6]. Recent developments have been devoted to finding the best metal ratio in order to maximize advantages over drawbacks depending on the final application. Batteries using layers of LiCoO₂ have been firstly used but, due to the cost and the toxicity of Co, other transition metals have been incorporated [7]. For example, LiNixMnyCozO₂ batteries (NMC with $x + y + z = 1$) have shown a high capacity (up to 160 mAh g⁻¹) with a high midpoint voltage (*vs.* Li) of 3.8 V and a good balance between stability, cyclability, cost of the material and performance. This makes them one of the most successful LiB on the market (47 kilotons/year) just after the LiFePO₄ (LFP) system (65 kilotons/year) and before the original LiCoO₂ (LCO) system (39 kilotons/year) in 2016. However, there are still some limitations to the use of NMC batteries such as the toxicity, the use of non-abundant metal (Li) and the recycling processes [8]. Present processes are generally based on pyrometallurgical and hydrometallurgical treatments [9].

* Corresponding author: david.peralta@cea.fr;
michael.carboni@cea.fr

Our team has recently obtained Metal-Organic Frameworks (MOFs) from a solution of Nickel, Manganese and Cobalt species (ratio 1:1:1) that includes all the metals inside the structure with the same proportion [10] or just Mn [11] depending on the nature of the precipitating agent. MOFs consist of inorganic nodes (clusters) bound together by organic linkers. They have gained a lot of popularity mostly due to their high surfaces, tunable structures and abundant active sites [12]. MOFs have been proposed in many applications such as gas storage, heterogeneous catalysis or extraction and separation of metals or organics [13]. Recently, mainly due to their crystalline organisation, MOFs and their derivatives have also been used as electrode materials [14], precursors for electrode synthesis [15] or solid electrolytes [16]. In this way, we have recently proposed an iron-based MOF as a cheap conversion material for the negative electrode of lithium batteries. Electrochemical properties measured in coin cells have revealed a high capacity of 550 mAh g⁻¹ with good cyclability over the charge/discharge cycles [17]. Electrode materials can also be prepared from MOFs after heat treatment under air to convert the material into oxide [18]. Recently, MIL-88-Fe of formula Fe₃O(H₂O)₂Cl(BDC)₃·nH₂O (BDC for benzene dicarboxylate), was chosen as a template to prepare a porous α -Fe₂O₃. This material shows an interesting capacity of 911 mAh g⁻¹ and good stability after 50 cycles at a rate of 0.2 °C [19]. Reduced transition metal which can be obtained by thermal treatment of MOF [20] under an inert atmosphere has also shown great potential for energy storage application [21]. As an example, exfoliated transition metal carbides and carbonitrides (MXene such as Ti₂AlC or V₂AlC) have been evaluated as Li⁺ intercalation electrodes in LiBs [22].

Here we propose to evaluate a MOF composed of Ni, Mn and Co coordinated to the BTC linker (BTC for trimesic acid), synthesized in our previous work, as anode materials for LiBs [10]. This material stabilizes inside its structure the three metals with a 1:1:1 ratio. The corresponding oxide and reduced materials, obtained after a heat treatment under air or argon respectively, have also been synthesized. The three materials have been characterized and the electrochemical capacities in coin cells have revealed a capacity of 690 and 190 mAh g⁻¹ after 50 cycles at 15 mA g⁻¹ respectively for the MOF and the oxide. The corresponding reduced form has nevertheless shown no electrochemical capacity.

2 Experimental section

2.1 Synthesis

Reagents were purchased from *Sigma-Aldrich* and were used as received without further purification. TGA was measured in a Mettler-Toledo TG with an auto-sampler. A FEI Quanta 200 environmental scanning electron microscope, equipped with an Everhart-Thornley Detector (ETD) and a Backscattered Electron Detector (BSED), was used to record images with an acceleration voltage of 30 kV under high vacuum conditions. PXRD patterns were obtained with a Bruker D8 Advance diffractometer using a

Cu anode delivering an x-ray beam of wavelength 1.542 Å. FTIR spectra were recorded with a Perkin Elmer 100 spectrometer between 380 and 4000 cm⁻¹ using an ATR crystal with 4 cm⁻¹ resolution. *Ex situ* XRD patterns were obtained by protecting the sample from air and moisture by using a *Kapton*[®] polyimide film. More precisely, the cycled coin cells are dismantled into a glove box. Anode electrodes are then removed and washed with Dimethyl Carbonate (DMC) in order to remove all residual salts. Then electrodes are fixed on glass supports and samples are then protected from air with a *Kapton*[®] polyimide film. The MOF was synthesized from a reported protocol [10]. In summary, 1 equivalent of each metal ([Ni(NO₃)₂ · 6H₂O], [Mn(NO₃)₂ · 9H₂O] and [Co(NO₃)₂ · 6H₂O]) are solubilized in DMF. To this solution, three equivalents of Trimesic acid were added and transferred to a Parr Bomb. The reaction was performed in solvothermal conditions at 120 °C for 2 days in an oven to obtain a crystalline pink material. Then the mixture was centrifuged, the supernatant was isolated and the precipitate was washed 3 times with DMF, 3 times with EtOH to eliminate any residual trace of DMF and finally dried overnight in an oven at 80 °C. The corresponding oxide was obtained by a heat treatment under air at 1000 °C during 12 h whereas the reduced form was obtained with a 1000 °C heat treatment under inert gas (argon) during 12 h.

2.2 Electrochemical characterizations

Coin cell assembly was carried out in an argon-filled MBraun glove box using metallic lithium foil as counter and reference electrode and Celgard[®] 2400 and Viledon[®] (*Freudenberg*) as separator, the latter soaked with a 1M solution of LiPF₆ in a 1:1 volume mixture of Ethylene Carbonate (EC) and Dimethyl Carbonate (DMC) (UBE), serving as electrolyte. Galvanostatic cycling was performed using an Arbin BT-2000. Composite electrodes for the electrochemical characterization were prepared by mixing Active Material (AM), Super P[®] (SP; *Imerys*) and Poly (Vinylidene difluoride) (PVdF, SOLEF[®] 5130; *Solvay*), in N-Methyl-2-Pyrrolidone (NMP; *Sigma-Aldrich*). The overall weight ratio was 40/40/20 (AM/SP/PVdF). The slurry was coated on copper foil, serving as a current collector, and after pre-drying, disk-shaped electrodes were punched, having an average active material mass loading of about 1 mg cm⁻². The electrodes were subsequently pressed at 10 tons for 10 s, and then, all the electrodes were dried at 80 °C for 48 h under vacuum. Since lithium foil served as a counter and reference electrode, all potential values given herein refer to the Li⁺/Li⁰ redox couple.

3 Results and discussion

3.1 Characterizations

The reaction between the trimesic acid and the 3 metals (Co, Ni and Mn in the ratio 1:1:1) in DMF leads to a pink crystalline material after 2 days at 120 °C.

The material is then washed thoroughly and dried. The metal ratio is confirmed by ICP-MS after the MOF

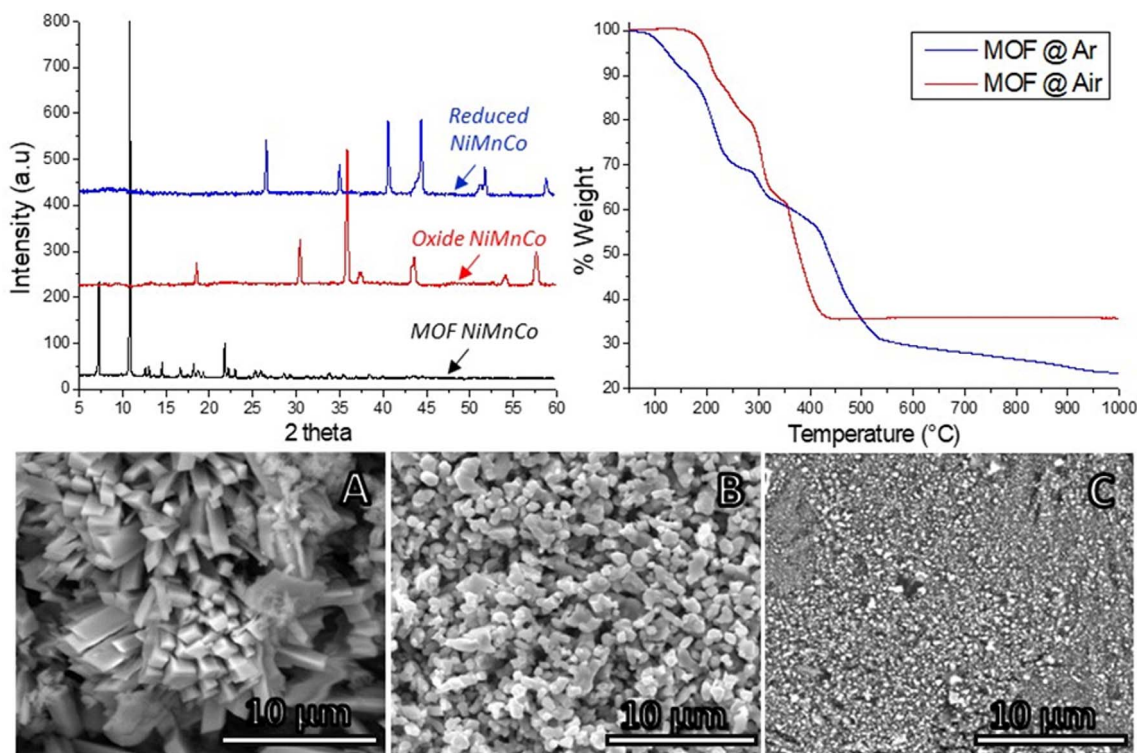


Fig. 1. (Top) left – PXRD analyses of the MOF, oxide and reduced forms; right – TGA of the MOF under air and argon. (bottom) SEM images of the MOF (A), oxide (B) and reduced MOF (C).

digestion and by EDX analysis on the material [10]. Previous analyses suggest the incorporation of all the metals inside the structure of the MOF and the structure guide of the cobalt in the morphology of the final product [10]. The IR spectra of this material and the BTC ligand are shown in Figure S1 and are consistent with the coordination of the metals to the ligand as reported by Gan *et al.* [23]. The characteristic bands of the protonated carboxyl groups of the BTC ($\nu\text{OH} = 3066\text{ cm}^{-1}$, $\nu\text{C}=\text{O} = 1690\text{ cm}^{-1}$) are absent in the IR spectrum of the MOF and new bands are observed attributed to the vibration of COO^- (1608 , 1438 and 1369 cm^{-1}). The conversion under heat treatment has been made under air or argon to form its oxidized and pyrolysed derivatives respectively. These materials have then been characterized by PXRD, TGA and SEM analyses prior to being tested as electrode material in a coin cell.

The MOF NiMnCo has revealed a few sharp peaks according to the formation of a material that combined the three metals in the structure [10]. The corresponding oxide also exhibits sharp peaks on its PXRD pattern between 15 and 60 degrees typical of a crystalline oxide. This pattern corresponds to the formation of NiMnCoO_4 with a space group $\text{Fd}\bar{3}\text{m}$ (Fig. 1 – top, left). Peak duplication can be observed in this pattern and is explained by the presence of impurities due to an excessive amount of cobalt in the host structure as previously reported [24]. The TGA profile is consistent with the formation of this oxide material by the thermal decomposition of the rehydrated MOF NiMnCo with the formula $\text{NiMnCo}(\text{BTC})_2 \cdot 6\text{H}_2\text{O}$ (Fig. 1 – top, right). The two first decomposition steps

correspond to the evaporation of free and adsorbed water molecules until 250 °C (20% weight loss). From 250 °C to 420 °C, the degradation of the organic framework occurs in two subsequent processes (45% weight loss) which leads to a residual and stable inorganic oxide compound (35% of the total weight). These results are in good accordance with the degradation of $\text{NiMnCo}(\text{BTC})_2 \cdot 6\text{H}_2\text{O}$ to NiMnCoO_4 . The thermal treatment of the MOF under an inert atmosphere shows a similar behaviour with the elimination of water until 250 °C (30% weight loss) followed by the decomposition of the framework until 550 °C (40% weight loss). Then a slow pyrolysis until 1000 °C (5% weight loss) is observed, probably due to the carbonization of the organic ligand associated with an increase of C/O ratio or to the reduction of the oxide material to the reduced form under argon. Here, a higher amount of water is observed inside the material, compared to the previous analysis under air showing that the material is very hygroscopic. Starting from $\text{NiMnCo}(\text{BTC})_2 \cdot 9\text{H}_2\text{O}$, the MOF-derived material can be noted as CoNiMnCx (with x ranging from 10 to 6 from 550 °C to 1000 °C). PXRD analysis indicates that no trace of the NiMnCoO_4 oxide appears in this material.

The structure of the three materials was analysed by SEM and the corresponding images are depicted in Figure 1-bottom. The SEM image of MOF NiMnCo indicates the presence of highly crystalline structures in rod shapes with dimensions of around 10 μm (Fig. 1A). The corresponding oxide (Fig. 1B) exhibits small and regular particles of around 1 μm size, suggesting that materials keep some organisation during the thermal conversion to form

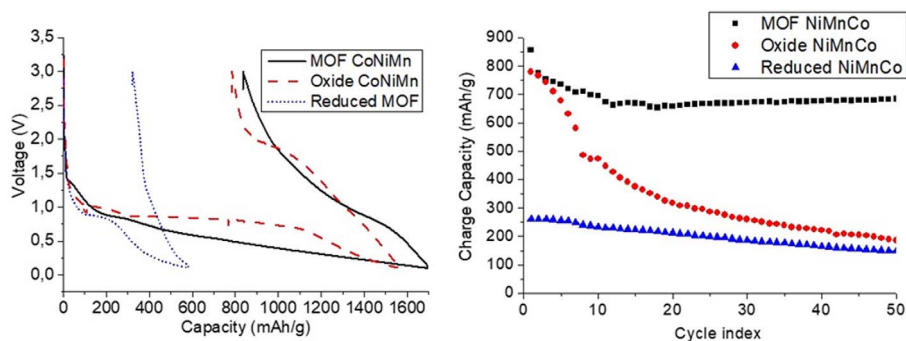


Fig. 2. First charge and discharge (left) and cycle life (right) of the 3 materials.

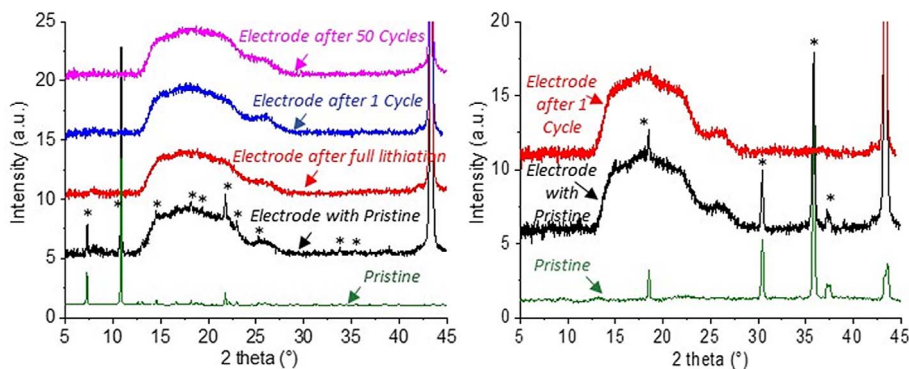


Fig. 3. *Ex situ* XRD patterns of MOF (left) and oxide (right). Asterisks highlight the MOF and oxide diffraction peaks.

NiMnCoO₄. In contrast, the SEM image of the corresponding pyrolysed material does not show any specific shape (Fig. 1C). Only very small and non-regular particles are observed. Transition metal carbides are indeed known to be polydispersed during the carbonization process [19].

2.3 Electrochemical performance

The electrochemical performances of the three materials have been evaluated in half-coin cells. Galvanostatic charge-discharge curves of MOFs electrodes at a current density of 15 mA g⁻¹ are exhibited in Figure 2-left. The first delithiation of the pyrolysed material corresponds to a quite low specific capacity (~250 mAh g⁻¹) which could be mainly attributed to the contribution of carbon additive in this voltage window (contribution of the Super P[®] carbon is of 150 mAh g⁻¹ after 15 charge/discharge cycles (Fig. S3)). On the contrary, the other materials show some high capacity of 800 mAh g⁻¹ during their delithiation. The MOF NiMnCo has a first lithiation capacity of 1690 mAh g⁻¹ with an average voltage of 0.5 V. The main part of the capacity is observed between 1 V and 0.1 V with a large hysteresis. The specific capacity in delithiation is 860 mAh g⁻¹ with an average voltage of 1.2 V that increases almost linearly. A very similar trend is observed with the NiMnCo oxide material even if the average voltage is slightly higher (0.7 V in lithiation and 1.4 V in delithiation). Figure 2-right represents the capacity of each material as a function of the cycle number. The electrochemical

performances of MOF NiMnCo are very stable with still 685 mAh g⁻¹ after 50 cycles. However, the capacity of the NiMnCo oxide decays quickly from 780 mAh g⁻¹ to 185 mAh g⁻¹ after 50 cycles. The shape of the galvanostatic curves suggests that conversion mechanisms are involved. Moreover, as previously reported, the structure of NiMnCoO₄ presents structural impurities due to the presence of Co ions in the host structure that affects the lithium ions intercalation/de-intercalation [24].

Ex situ XRD has been performed in order to follow the structure evolution during cycling (Fig. S2). Figure 3-left represents the XRD of the MOF NiMnCo at different stages of cycling. Three different coin cells have been made with MOF NiMnCo-based electrodes. One is stopped after the first lithiation, a second after a full cycle and the last after 50 cycles. To allow easier comparison between XRD patterns and to take into account the Kapton[®] film signal in the interpretation, a pristine electrode has also been characterized. On the pristine electrode, the different asterisks index the original diffraction peaks of the material (the strong peak at 43° is due to the copper current collector). It is important to note that the MOF NiMnCo could be identified even if the Kapton[®] film signal is quite intense in the 12°–25° area. Another interesting point is that the MOF structure was maintained during the cell manufacturing steps especially, after the calendaring step at 7 tons cm⁻². After cycling, the cell was dismantled and the electrode was recovered, cleaned and characterized. No XRD peak corresponding to the initial material could

be identified on all cycled electrodes. It is clear that the MOF structure is not maintained at the end of the first lithiation and the material is not recovered at the end of the first cycle. A similar experience has been made with the NiMnCo oxide (Fig. 3-right). The same conclusion could be drawn, initial XRD peaks could not be found after the first discharge.

The *Ex situ* XRD patterns are in good agreement with the hypothesis of the conversion mechanism of the two materials. In such a mechanism, the lithiation would lead to the reduction of the active material in metallic nanoparticles.

However, even if both materials are reduced following the same phenomena, the cycle life of the reduced metals generated by the MOF is clearly better than the oxide one. In fact, because both materials have the same metal ratio, and the same initial capacity (no organic ligand contribution), it is expected that electrochemical performances will be similar. However, this is not the case and the only possible interpretation is that the reduced materials morphology is different. We assume that the particle size of the reduced MOF at the end of the reduction is smaller than the oxides. In the case of the MOF NiMnCo, all metal clusters are separated by organic ligands which can lead to very small and isolated metallic particles at the end of the reduction process [25]. Inversely, in the case of the oxide, all atoms are very close to each other due to the oxygen bonds. SEM pictures of electrodes (MOF and oxide) before and after 1 cycle confirm this hypothesis. MOF particles can no longer be observed at the end of the first cycle (Fig. S4). Due to the better dispersion in smaller particles obtained by the MOF reduction, the electrochemical performances, and notably the cycle life, seem to be improved.

4 Conclusion

A MOF and its oxidized and reduced derivatives have been developed and have demonstrated some interesting electrochemical performances. This hybrid material can integrate three metals (Ni, Mn and Co) in its structure with a ratio of 1:1:1. The thermal treatment under air was conducted to the formation of a crystalline oxide, while under inert conditions, a crystalline reduced material was obtained. Only the MOF and the oxide have shown significant electrochemical activities but both materials exhibit a conversion mechanism during cycling and present high charge and discharge capacities. Generally, oxide materials are known to allow high capacity due to the conversion mechanism. However, our MOF has revealed a higher capacity and more importantly better stability than the oxide during the charge-discharge cycling experiments. We highlight that well-dispersed and smaller metallic particles related to the reduction of MOF metal clusters allow us to achieve a better cycle life.

Both materials have high capacities and prove that a real interest exists in conducting research on MOF materials for Li-ion applications. In the future, the real challenge for the use of MOF in batteries will be to find a framework that can support a lower potential with capacities as high as

those observed with the NiMnCo MOF or the NiMnCo oxide.

Acknowledgments. The authors are grateful to Joseph Lautru for SEM analyses and Halima Toumkara for her help with the electrochemical experiments. MC, TG and DP thank the CEA for financial support with the Bottom-up project (*Engin Molva*).

Conflicts of interest

There are no conflicts to declare.

Supplementary material

The Supplementary material of this article is available at <https://stet-review.org/10.2516/stet/2023031/olm>.

Figure S1: FT-IR spectra of BTC (top) and MOF NiMnCo (bottom).

Figure S2: Galvanostatic curves of cells used for ex situ XRD of the MOF NiMnCo (top) and the oxide (bottom).

Figure S3: Cycling performance of the Carbon SuperP.

Figure S4: SEM pictures of electrodes (MOF and oxide) before and after 1 cycle.

References

- 1 Chu S., Majumdar A. (2012) Opportunities and challenges for a sustainable energy future, *Nature* **488**, 294–303.
- 2 Antonakakis N., Chatziantoniou I., Filis G. (2017) Energy consumption, CO₂ emissions, and economic growth: an ethical dilemma, *Renew. Sustain. Energy Rev.* **68**, 808–824.
- 3 Canepa P., Sai Gautam G., Hannah D.C., Malik R., Liu M., Gallagher K.G., Persson K.A., Ceder G. (2017) Odyssey of multivalent cathode materials: open questions and future challenges, *Chem. Rev.* **117**, 4287–4341.
- 4 Goodenough J.B., Kim Y. (2010) Challenges for rechargeable Li batteries, *Chem. Mater.* **22**, 587–603.
- 5 Divya K.C., Østergaard J. (2009) Battery energy storage technology for power systems—an overview, *Electr. Power Syst. Res.* **79**, 511–520.
- 6 Mizushima K., Jones P.C., Wiseman P.J., Goodenough J.B. (1980) Li_xCoO₂ (0 < x < 1): a new cathode material for batteries of high energy density, *Mater. Res. Bull.* **15**, 783–789.
- 7 Zhang H., Mao C., Li J., Chen R. (2017) Advances in electrode materials for Li-based rechargeable batteries, *RSC Adv.* **7**, 33789–33811.
- 8 Lv W., Wang Z., Cao H., Sun Y., Zhang Y., Sun Z., (2018) A critical review and analysis on the recycling of spent lithium-ion batteries, *ACS Sustain. Chem. Eng.* **6**, 1504–1521.
- 9 Dutta T., Kim K.-H., Deep A., Szulejko J.E., Vellingiri K., Kumar S., Kwon E.E., Yun S.-T. (2018) Recovery of nanomaterials from battery and electronic wastes: a new paradigm of environmental waste management, *Renew. Sustain. Energy Rev.* **82**, 3694–3704.
- 10 Perez E., Navarro Amador R., Carboni M., Meyer D. (2016) In-situ precipitation of metal-organic frameworks from a simulant battery waste solution, *Mater. Lett.* **167**, 188–191.

- 11 Perez E., Andre M.-L., Navarro Amador R., Hyvrard F., Borrini J., Carboni M., Meyer D. (2016) Recovery of metals from simulant spent lithium-ion battery as organophosphate coordination polymers in aqueous media, *J. Hazard. Mater.* **317**, 617–621.
- 12 Yang X.-Y., Chen L.-H., Li Y., Rooke J.C., Sanchez C., Su B.-L. (2017) Hierarchically porous materials: synthesis strategies and structure design, *Chem. Soc. Rev.* **46**, 481–558.
- 13 Furukawa H., Cordova K.E., O’Keeffe M., Yaghi O.M. (2013) The chemistry and applications of metal-organic frameworks, *Science* **341**, 1230444–1230444.
- 14 Du Z.-Q., Li Y.-P., Wang X.-X., Wang J., Zhai Q.-G. (2019) Enhanced electrochemical performance of Li–Co-BTC ternary metal–organic frameworks as cathode materials for lithium-ion batteries, *Dalton Trans.* **48**, 2013–2018.
- 15 Ma Y., He J., Kou Z., Elshahawy A.M., Hu Y., Guan C., Liang X., Wang J. (2018) MOF-derived vertically aligned mesoporous Co_3O_4 nanowires for ultrahigh capacity lithium-ion batteries anodes, *Adv. Mater. Interfaces* **5**, 1800222.
- 16 Wu J.-F., Guo X. (2019) MOF-derived nanoporous multi-functional fillers enhancing the performances of polymer electrolytes for solid-state lithium batteries, *J. Mater. Chem. A* **7**, 2653–2659.
- 17 Cagnet M., Gutel T., Peralta D., Maynadié J., Carboni M., Meyer D. (2017) Communication—iron(II)-benzene phosphonate coordination polymers as an efficient active material for negative electrode of lithium-ion batteries, *J. Electrochem. Soc.* **164**, A2552–A2554.
- 18 Xia W., Mahmood A., Zou R., Xu Q. (2015) Metal–organic frameworks and their derived nanostructures for electrochemical energy storage and conversion, *Energy Env. Sci* **7**, 1837–1866.
- 19 Xu X., Cao R., Jeong S., Cho J. (2012) Spindle-like mesoporous $\alpha\text{-Fe}_2\text{O}_3$ anode material prepared from MOF template for high-rate lithium batteries, *Nano Lett.* **12**, 4988–4991.
- 20 Yu Z., Bai Y., Zhang S., Liu Y., Zhang N., Wang G., Wei J., Wu Q., Sun K., Appl A.C.S. (2018) Metal–organic framework-derived $\text{Co}_3\text{ZnC}/\text{Co}$ embedded in nitrogen-doped carbon nanotube-grafted carbon polyhedra as a high-performance electrocatalyst for water splitting, *Mater. Interfaces* **10**, 6245–6252.
- 21 Zhong Y., Xia X., Shi F., Zhan J., Tu J., Fan H.J. (2016) Transition metal carbides and nitrides in energy storage and conversion, *Adv. Sci.* **3**, 1500286.
- 22 Naguib M., Come J., Dyatkin B., Presser V., Taberna P.-L., Simon P., Barsoum M.W., Gogotsi Y. (2012) MXene: a promising transition metal carbide anode for lithium-ion batteries, *Electrochem. Commun.* **16**, 61–64.
- 23 Gan Q., He H., Zhao K., He Z., Liu S. (2018) Morphology-dependent electrochemical performance of Ni-1,3,5-benzenetricarboxylate metal-organic frameworks as an anode material for Li-ion batteries, *J. Colloid Interface Sci.* **530**, 127–136.
- 24 Zhao H., Liu L., Hu Z., Sun L., Han S., Liu Y., Chen D., Liu X. (2016) Neutron diffraction analysis and electrochemical performance of spinel $\text{Ni}(\text{Mn}_{2-x}\text{Co}_x)\text{O}_4$ as anode materials for lithium ion battery, *Mater. Res. Bull.* **77**, 265–270.
- 25 Lee H.H., Lee J.B., Park Y., Park K.H., Okyay M.S., Shin D.-S., Kim S., Park J., Park N., An B.-K., Jung Y.S., Lee H.-W., Lee K.T., Hong S.Y., Appl A.C.S. (2018) Coordination polymers for high-capacity Li-ion batteries: metal-dependent solid-state reversibility, *Mater. Interfaces* **10**, 22110–22118.